Mobility and Decay Dynamics of Charge Carriers in One-Dimensional Selenium van der Waals Solid

Bhaskar, Prashant; Achtstein, Alexander W.; Diedenhofen, Silke L.; Siebbeles, Laurens D.A.

DOI
10.1021/acs.jpcc.7b05183

Publication date
2017

Document Version
Final published version

Published in
The Journal of Physical Chemistry C

THE JOURNAL OF PHYSICAL CHEMISTRY C

Article

pubs.acs.org/JPCC

Mobility and Decay Dynamics of Charge Carriers in One-Dimensional Selenium van der Waals Solid

Prashant Bhaskar,*[,†] Alexander W. Achtstein,[†,‡] Silke L. Diedenhofen, and Laurens D. A. Siebbeles*

Optoelectronic Materials Section, Department of Chemical Engineering, Delft University of Technology, Van der Maasweg 9, 2629 HZ Delft, The Netherlands

ABSTRACT: Trigonal selenium is a semiconducting van der Waals solid that consists of helical atomic chains. We studied the mobility and decay dynamics of excess electrons and holes moving along the selenium chains. Excess charge carriers were generated by irradiation of powdered selenium with 3 MeV electron pulses. Their mobility and decay via trapping or recombination was studied by time-resolved microwave conductivity measurements as a function of temperature. The mobility of charge carriers along the Se chains is at least ca. 0.5 $cm^2 \cdot V^{-1} \cdot s^{-1}$ at room temperature. Charges decay predominantly by trapping at defects. The appreciable mobility, together with the potential for large-scale production of Se wires by liquid exfoliation, makes this material of great interest for use in nanoelectronics.

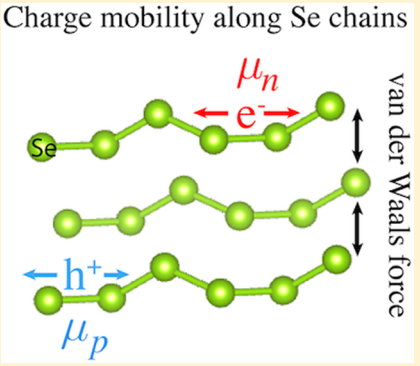

INTRODUCTION

van der Waals solids attract a great deal of interest, due to the possibility of preparing single layers or stacks of two-dimensional (2D) semiconductor sheets.[1−3] Electronic quantum confinement perpendicular to the plane of a sheet allows one to tune the optoelectronic properties by varying the number of stacked sheets. Recent developments in large-scale production of 2D sheets via liquid exfoliation offer promising prospects for optoelectronic applications, in contrast to small-scale mechanical exfoliation[4−6] or controlled solution-phase chemical synthesis.[7]

In nanoelectronics, one-dimensional (1D) wires are also of interest. Solution-processable nanowires have been studied in the form of conjugated organic molecular chains (polymers)[8−13] or as colloidal semiconductor nanorods/nanowires.[14] Interestingly 1D van der Waals solids also exist, such as trigonal selenium (Se) and tellurium (Te).[15] Until now, only a few studies on the optoelectronic properties of these 1D van der Waals solids have been reported, including calculations of electronic band structure[16−18] and measurements of photoconductivity,[19,20] magnetoconductivity,[21] magnetoabsorption,[18] and electroreflectance.[22] Charge carrier mobilities from 0.1 up to 40 $cm^2 \cdot V^{-1} \cdot s^{-1}$ were found for (photo)doped trigonal Se.[19−21,23] In these measurements, the high doping densities could have led to trap filling, which increases the mobility compared to that at low charge carrier density.

The aim of the present study is to provide insight into the mobility and charge decay dynamics via trapping or recombination in trigonal Se at varying charge carrier density, similar to our previous work on 2D black phosphorus.[24] Possible negative effects of backscattering of charges at the ends of Se chains on the mobility are discussed, using the theoretical model of Prins et al.[25]

EXPERIMENTAL METHODS

Pellets of trigonal Se from Sigma−Aldrich with purity ≥99.999% were powdered by use of a pestle and mortar. The trigonal crystal structure was confirmed from Raman spectroscopy on a Renishaw inVia system in backscattering configuration with an excitation wavelength of 514 nm.

To study the dynamics of excess charge carriers, the Se powder was introduced into a microwave conductivity measurement cell with dimensions suitable for frequencies in the K_a band (27−38 GHz), similar to our previous studies.[24] High-energy (3 MeV) electron pulses from a van de Graaff accelerator were used to generate excess electrons and holes in the sample. The high-energy electrons pass through the sample and lose energy by generating a close to uniform distribution of electron−hole pairs along their tracks without inducing net charging in the sample. During the 3 MeV electron pulse, electron−hole pairs are generated with number density per unit time, G, given by the ratio of the known energy-transfer rate (radiation dose per unit time) from the electron pulse to the sample and the energy required for formation of an electron−hole pair. The radiation dose in the Se sample, D_{Se}, was obtained from a reference measurement on benzene (Bz) according to $D_{Se} = D_{Bz}(N_{e,Se}\rho_{Se}M_{Bz}/N_{e,Bz}\rho_{Bz}M_{Se})$, where N_e, ρ, and M are respectively the number of electrons per atom/molecule, mass density, and atomic/molecular mass for Se or Bz.[24,26] The electron−hole pair formation energy, E_p, was estimated from the empirical formula provided by Alig et al.,[27] which is given by $E_p = 2.73E_g + b$, where $b = 0.5$ eV and E_g =

Received: May 29, 2017
Revised: July 21, 2017
Published: August 8, 2017

DOI: 10.1021/acs.jpcc.7b05183
J. Phys. Chem. C 2017, 121, 18917−18921

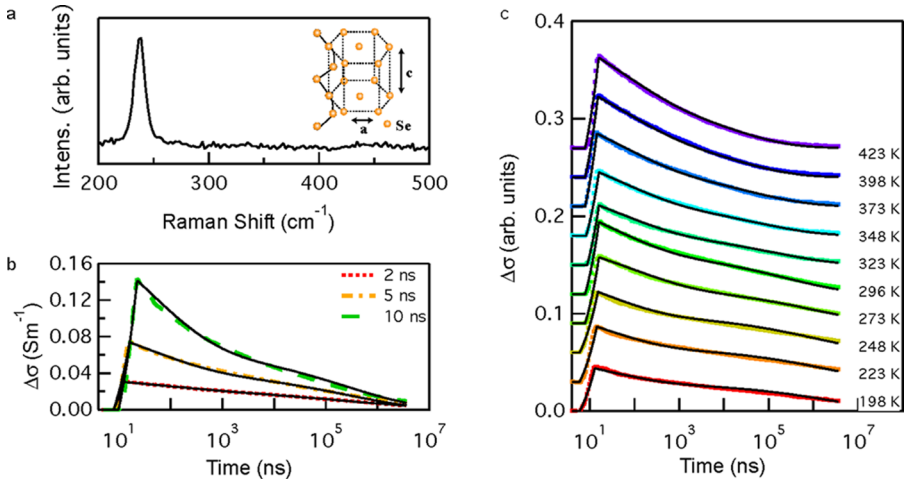

Figure 1. (a) Raman spectrum exhibiting a peak at 237 cm^{-1}, characteristic for helical Se chains in the trigonal phase with a crystal structure as shown in the inset. (b) Transient microwave conductivity due to excess charge carriers in Se at room temperature, measured for different durations of the 3 MeV electron pulse (colored curves) and obtained from theoretical modeling (drawn black curves). (c) Transient conductivity obtained with a 5 ns electron pulse for different temperatures, shown with vertical offsets for clarity.

1.9 eV,[18] the band gap of trigonal Se. The density of generated electron−hole pairs is given by the ratio D_{Se}/E_p.

The transient conductivity, $\Delta\sigma(t)$, due to excess charge carriers is obtained from the measured change of microwave power reflected from the cell, according to $\Delta P(t)/P = -A\Delta\sigma(t)$, where A is a sensitivity factor that depends on the cell dimensions and dielectric constant of the sample.[28] The transient conductivity is equal to $\Delta\sigma(t) = e[\mu_n n(t) + \mu_p p(t)]$, where e is the elementary charge, μ_n and μ_p are mobilities of electrons and holes, and $n(t)$ and $p(t)$ are transient densities of excess electrons and holes, respectively.

RESULTS AND DISCUSSION

Structural Characterization. The crystal structure of the powdered Se sample was characterized by Raman spectroscopy (see Experimental Methods). The measured Raman spectrum in Figure 1a shows a peak at 237 cm^{-1}, which is characteristic for the trigonal phase consisting of helical chains of Se atoms.[15,29,30] Other phases of Se (α-monoclinic or vitreous) are known to exhibit Raman shifts in the range 250−256 cm^{-1},[15] which are not observed in Figure 1a. From this we infer that our sample predominantly consists of helical Se chains in the trigonal phase, as shown in the inset of Figure 1a.

Transient Microwave Conductivity Measurements. The powdered trigonal Se sample was contained in a rectangular microwave cell suitable for conductivity detection near 30 GHz (see Experimental Methods). The sample was irradiated with pulses of 3 MeV electrons that lose energy along their path through the sample via impact ionization. This leads to production of secondary, tertiary, etc., excess electrons and holes with a close-to-uniform spatial distribution. The incident 3 MeV electrons lose only part of their energy and leave the sample, so that net charging of the sample does not occur.

Figure 1b shows the transient microwave conductivity obtained for pulse durations as indicated. The conductivity increases during the pulse due to generation of mobile electrons and holes in the sample. The conductivity at the end of the electron pulse increases with its duration, which reflects that the density of the produced electrons and holes is higher for a longer pulse. The charge carrier decay occurs by trapping at defects or by electron−hole recombination. It can be seen that the conductivity becomes shorter-lived for longer pulse duration, which is caused by faster higher-order recombination of electrons and holes at higher density.

Figure 1c shows the temperature dependence of conductivity in the range 198−423 K. The conductivity transients are plotted with vertical offsets for clarity. The conductivity at the end of the 3 MeV electron pulse increases with temperature and the decay kinetics becomes faster.

Theoretical Modeling. The transient microwave conductivity is given by $\Delta\sigma(t) = e[\mu_n n(t) + \mu_p p(t)]$, where μ_n or μ_p is the electron or hole mobility, $n(t)$ or $p(t)$ is the electron or hole density, and e is the elementary charge. Charge mobilities and decay kinetics were obtained from fitting a theoretical model to the measured conductivity. Electron and hole densities are described by the following differential equations:

$$\frac{dn(t)}{dt} = G_{pulse}\phi_n - \frac{\beta_n(k_{1n}t)^{\beta_n}}{t}n(t) - k_2 n(t)p(t) \quad (1)$$

$$\frac{dp(t)}{dt} = G_{pulse}\phi_p - \frac{\beta_p(k_{1p}t)^{\beta_p}}{t}p(t) - k_2 p(t)n(t) \quad (2)$$

In eqs 1 and 2, the first term contains the generation of electrons and holes with rate $G_{pulse} = G[\Theta(t) - \Theta(t - t_{pulse})]$, where Θ is the Heaviside function making it nonzero only during the 3 MeV electron pulse. Furthermore, ϕ_n and ϕ_p denote the fraction of charges surviving from direct trapping or geminate electron−hole recombination during the 3 MeV electron pulse. The second terms in eqs 1 and 2 represent first-order electron (hole) trapping with characteristic rate k_{1n} or k_{1p}, which by themselves yield a stretched-exponential decay given by $n(t) = n(t = 0)\exp[(-k_1 t)^{\beta}]$.[31] Such stretched-exponential decay can occur from charges that need to diffuse to traps with a characteristic time $1/k_{1n}$ or $1/k_{1p}$, followed by irreversible trapping. In that case of diffusion-limited trapping, the parameter $\beta = d/(d + 2)$, where d is the dimensionality of the medium.[31,32] The third terms in eqs 1 and 2 bring into account second-order radiative recombination of electrons and holes with rate constant k_2.

The coupled differential equations (eqs 1 and 2) were solved by a fourth-order Runge−Kutta method. The measured

DOI: 10.1021/acs.jpcc.7b05183
J. Phys. Chem. C 2017, 121, 18917−18921

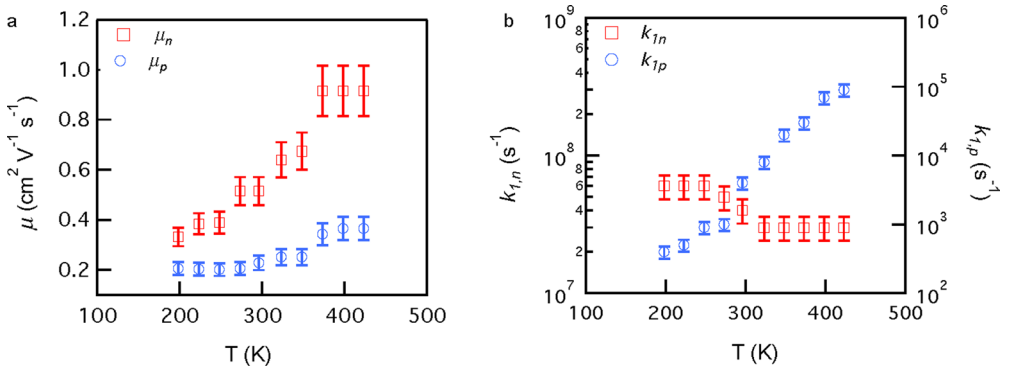

Figure 2. (a) Temperature dependence of (a) measured microwave mobilities of electrons and holes and (b) their trapping rates.

conductivity was modeled by fitting a constrained set of shared parameters $\phi_{n,p}$, $\beta_{n,p}$, and k_2 for all the experimental data, while the charge mobilities μ_n and μ_p and first-order decay rates k_{1n} and k_{1p} were allowed to vary with temperature. The model fits our experimental data as shown in Figure 1b,c. In the first instance, we included the recombination of free charges with trapped charges. It turned out that mutual recombination of the free charges with rate constant (k_2) is much more efficient than recombination of free charges with trapped charges. Consequently, recombination of free charges with trapped charges was ignored in eqs 1 and 2.

The averaged conductivity transients were found to be independent of the number of 3 MeV electron pulses used. Hence, all charges recombine between successive electron pulses (with repetition rate of ~1 s^{-1}) and charge accumulation does not affect our results.

Initial Yield and Mobility of Charge Carriers. We found from our fits that one type of charge carrier becomes trapped much faster than the other. Following a previous report on efficient electron trapping in Se, we attribute the charge carriers that are trapped fastest to electrons.[20] We found electron survival fractions equal to $\phi_n = 0.11 \pm 0.01$, 0.36 ± 0.03, and 0.57 ± 0.06 for 2, 5, and 10 ns pulse duration, respectively. The increase of survival fraction with pulse duration, or equivalently with initial electron density, can be attributed to a larger fraction of traps being filled at higher initial electron density. The fits yielded $\phi_p = 1$, which implies that all holes survive from trapping during the 3 MeV electron pulse. Nevertheless, charge neutrality is always obeyed, since the trapped charges are immobile only within the sample.

The fits yielded $\beta_n = \beta_p = 0.30 \pm 0.05$, corresponding to 1D charge transport ($d = 1$). In agreement with this, the helical chains in trigonal Se are held together by weak van der Waals forces, causing transport along the chains to be much more efficient than from one chain to another, which leads to (almost) 1D charge transport.

The 1D mobilities of electrons and holes moving along the Se chains were found to be $\mu_n = 0.52 \pm 0.06$ cm^2·V^{-1}·s^{-1}and $\mu_p = 0.23 \pm 0.03$ cm^2·V^{-1}·s^{-1} at room temperature. The mobilities increase with temperature as shown in Figure 2a. The increase in mobility with temperature may be due to scattering on static structural defects or charged impurities that can be surpassed by thermal activation.[33] At elevated temperature, the mobilities of electrons and holes tend to saturate. This can be attributed to a more prominent role of scattering on phonons, which has a reducing effect on the mobility.

The microwave mobilities in Figure 2a, obtained from the measured conductivity data in Figure 1, can be limited by scattering of charges at the ends of Se chains. In that case, the intrachain mobility of charge carriers, μ_{intra} (that would be obtained in absence of such scattering), can be related to the measured alternating current (ac) mobility of charges, μ_{ac}, moving on a chain with length L in an ac electric field oscillating with radian frequency ω, according to

$$\mu_{ac} = 8\mu_{intra} \sum_{j=0}^{\infty} \frac{c_j^{-2}}{\left(\frac{\mu_{intra} k_B T}{eL^2\omega}\right)^2 c_j^4 + 1} \quad (3)$$

with $c_j = 2\pi(j + {}^1/_2)$.[25] Figure 3 shows the ac mobility at the experimental frequency of 30 GHz, calculated according to eq

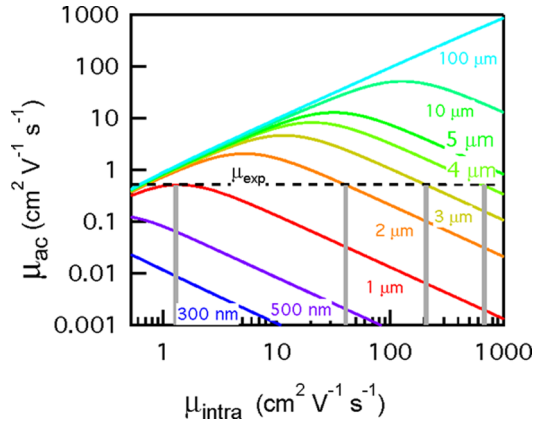

Figure 3. Microwave mobility as a function of intrachain mobility for Se chains with lengths as indicated. The dashed horizontal line indicates a mobility of 0.5 cm^2·V^{-1}·s^{-1}, which is close to the experimental values for electrons and holes at room temperature.

3, as a function of μ_{intra} for chain lengths in the range 300 nm–100 μm. The dashed horizontal line denotes a mobility value of 0.5 cm^2·V^{-1}·s^{-1}, which is close to experimental results for electrons and holes at room temperature. It can be seen from Figure 3 that the Se chains should at least have a length of ~1 μm to reproduce the experimental mobility. For longer chains, the mobility can be higher than the measured value, since the latter can be limited by charge scattering at chain ends. Unfortunately, a quantitative analysis of the distribution of the lengths of atomically thin Se chains in bulk is not possible with available electronic microscopic techniques. Interestingly, for conjugated polymer chains, such as ladder-type poly(*p*-phenylene), the measured microwave mobility of 0.24 cm^2·V^{-1}·s^{-1} was found to be strongly restricted by scattering at

DOI: 10.1021/acs.jpcc.7b05183
J. Phys. Chem. C 2017, 121, 18917–18921

chain ends, while the intrachain mobility was as high as 600 $cm^2 \cdot V^{-1} \cdot s^{-1}$, as inferred from analysis of mobility data for a series of chain lengths.[25] Therefore, experiments on Se chains with well-defined length are needed to further establish the precise value of intrachain mobility.

Charge Decay by Trapping and Recombination. Figure 2b depicts the trapping rates for electrons and holes at different temperatures. The electron-trapping rate slightly decreases with temperature, while it increases strongly for holes. The reduction of the electron-trapping rate with temperature can be due to faster thermally activated release of electrons from shallow traps. The presence of shallow electron traps agrees with the thermally activated electron mobility in Figure 2a. The strong thermally activated trapping rate for holes suggests that they need to overcome a potential barrier to be trapped. The second-order electron−hole recombination rate is 10^{-13} $cm^3 \cdot s^{-1}$ and was found to be independent of temperature. This rate is likely due to relatively slow diffusion of charge carriers between different Se chains and therefore does not reflect the temperature dependence of intrachain charge mobility.

CONCLUSIONS

In conclusion, the 1D mobility of charge carriers along helical chains of Se in the trigonal phase is at least ca. 0.5 $cm^2 \cdot V^{-1} \cdot s^{-1}$ at room temperature, which is promising for applications in nanoelectronics. In addition, the fact that Se is a van der Waals solid offers prospects for large-scale production of isolated chains or bunches via liquid exfoliation.

AUTHOR INFORMATION

Corresponding Authors

*(P.B.) E-mail p.bhaskar@tudelft.nl.

*(L.D.A.S.) E-mail l.d.a.siebbeles@tudelft.nl.

ORCID

Prashant Bhaskar: 0000-0002-5805-9756

Laurens D. A. Siebbeles: 0000-0002-4812-7495

Present Address

‡(A.W.A.) Technische Universität Berlin, Institut für Optik and Atomare Physik, Straße des 17 Juni 135, D-10623 Berlin, Germany.

Author Contributions

†A.W.A. and P.B. contributed equally to this work.

Notes

The authors declare no competing financial interest.

ACKNOWLEDGMENTS

P.B. and L.D.A.S. thank The Netherlands Organisation for Scientific Research (NWO) for financial support. A.W.A. acknowledges DFG Project AC290/1. S.L.D. acknowledges the research programme of the Foundation for Fundamental Research on Matter (FOM), which is a part of The Netherlands Organisation for Scientific Research (NWO).

REFERENCES

(1) Zhang, W.; Wang, Q.; Chen, Y.; Wang, Z.; Wee, A. T. S. Van Der Waals Stacked 2D Layered Materials for Optoelectronics. *2D Mater.* **2016**, *3*, No. 022001, DOI: 10.1088/2053-1583/3/2/022001.

(2) Lin, Z.; McCreary, A.; Briggs, N.; Subramanian, S.; Zhang, K.; Sun, Y.; Li, X.; Borys, N. J.; Yuan, H.; Fullerton-Shirey, S. K.; et al. 2D Materials Advances: From Large Scale Synthesis and Controlled Heterostructures to Improved Characterization Techniques, Defects and Applications. *2D Mater.* **2016**, *3*, No. 042001.

(3) Ryder, C. R.; Wood, J. D.; Wells, S. A.; Hersam, M. C. Chemically Tailoring Semiconducting Two-Dimensional Transition Metal Dichalcogenides and Black Phosphorus. *ACS Nano* **2016**, *10*, 3900−3917.

(4) Nicolosi, V.; Chhowalla, M.; Kanatzidis, M. G.; Strano, M. S.; Coleman, J. N. Liquid Exfoliation of Layered Materials. *Science* **2013**, *340*, No. 1226419.

(5) Coleman, J. N.; Lotya, M.; O'Neill, A.; Bergin, S. D.; King, P. J.; Khan, U.; Young, K.; Gaucher, A.; De, S.; Smith, R. J.; et al. Two-Dimensional Nanosheets Produced by Liquid Exfoliation of Layered Materials. *Science* **2011**, *331*, 568−571.

(6) Niu, L.; Coleman, J. N.; Zhang, H.; Shin, H.; Chhowalla, M.; Zheng, Z. Production of Two-Dimensional Nanomaterials Via Liquid-Based Direct Exfoliation. *Small* **2016**, *12*, 272−293.

(7) Gates, B.; Mayers, B.; Cattle, B.; Xia, Y. Synthesis and Characterization of Uniform Nanowires of Trigonal Selenium. *Adv. Funct. Mater.* **2002**, *12*, 219−227.

(8) Xiao, C.; Zhao, G.; Zhang, A.; Jiang, W.; Janssen, R. A. J.; Li, W.; Hu, W.; Wang, Z. High Performance Polymer Nanowire Field-Effect Transistors with Distinct Molecular Orientations. *Adv. Mater.* **2015**, *27*, 4963−4968.

(9) Briseno, A. L.; Mannsfeld, S. C. B.; Jenekhe, S. A.; Bao, Z.; Xia, Y. Introducing Organic Nanowire Transistors. *Mater. Today* **2008**, *11*, 38−47.

(10) Zhou, Y.; Lei, T.; Wang, L.; Pei, J.; Cao, Y.; Wang, J. High-Performance Organic Field-Effect Transistors from Organic Single-Crystal Microribbons Formed by a Solution Process. *Adv. Mater.* **2010**, *22*, 1484−1487.

(11) Grozema, F. C.; Hoofman, R. J. O. M.; Candeias, L. P.; de Haas, M. P.; Warman, J. M.; Siebbeles, L. D. A. The Formation and Recombination Kinetics of Positively Charged Poly(Phenylene Vinylene) Chains in Pulse-Irradiated Dilute Solutions. *J. Phys. Chem. A* **2003**, *107*, 5976−5986.

(12) Grozema, F. C.; Siebbeles, L. D. A. Charge Mobilities in Conjugated Polymers Measured by Pulse Radiolysis Time-Resolved Microwave Conductivity: From Single Chains to Solids. *J. Phys. Chem. Lett.* **2011**, *2*, 2951−2958.

(13) Warman, J. M.; de Haas, M. P.; Dicker, G.; Grozema, F. C.; Piris, J.; Debije, M. G. Charge Mobilities in Organic Semiconducting Materials Determined by Pulse-Radiolysis Time-Resolved Microwave Conductivity: Π-Bond-Conjugated Polymers Versus Π−Π-Stacked Discotics. *Chem. Mater.* **2004**, *16*, 4600−4609.

(14) Krahne, R.; Morello, G.; Figuerola, A.; George, C.; Deka, S.; Manna, L. Physical Properties of Elongated Inorganic Nanoparticles. *Phys. Rep.* **2011**, *501*, 75−221.

(15) Minaev, V. S.; Timoshenkov, S. P.; Kalugin, V. V. Structural and Phase Transformations in Condensed Selenium. *J. Optoelectron. Adv. Mater.* **2005**, *7*, 1717−1741 (https://joam.inoe.ro/arhiva/pdf7_4/Minaev.pdf).

(16) Tutihasi, S.; Chen, I. Optical Properties and Band Structure of Trigonal Selenium. *Phys. Rev.* **1967**, *158*, 623−630.

(17) Treusch, J.; Sandrock, R. Energy Band Structures of Selenium and Tellurium (Kohn-Rostoker Method). *Phys. Status Solidi B* **1966**, *16*, 487−497.

(18) Stuke, J. Recent Progress in the Physics of Selenium and Tellurium. In *The Physics of Selenium and Tellurium*; Pergamon: 1969; pp 3−20; DOI: 10.1016/B978-0-08-013895-4.50004-0.

(19) Mort, J. Acoustoelectric Current Saturation in Trigonal Selenium. *Phys. Rev. Lett.* **1967**, *18*, 540−543.

(20) Mort, J. Transient Photoconductivity in Trigonal Selenium Single Crystals. *J. Appl. Phys.* **1968**, *39*, 3543−3549.

(21) Mell, H.; Stuke, J. Magnetoconductivity of Hexagonal Selenium Single Crystals. *Phys. Lett.* **1966**, *20*, 222−224.

(22) Weiser, G.; Stuke, J. Electroreflectance on Trigonal Selenium. *Phys. Status Solidi B* **1971**, *45*, 691−703.

(23) Luo, L.-B.; Yang, X.-B.; Liang, F.-X.; Jie, J.-S.; Li, Q.; Zhu, Z.-F.; Wu, C.-Y.; Yu, Y.-Q.; Wang, L. Transparent and Flexible Selenium Nanobelt-Based Visible Light Photodetector. *CrystEngComm* **2012**, *14*, 1942−1947.

DOI: 10.1021/acs.jpcc.7b05183
J. Phys. Chem. C 2017, 121, 18917−18921

(24) Bhaskar, P.; Achtstein, A. W.; Vermeulen, M. J. W.; Siebbeles, L. D. A. Radiatively Dominated Charge Carrier Recombination in Black Phosphorus. *J. Phys. Chem. C* **2016**, *120*, 13836−13842.
(25) Prins, P.; Grozema, F. C.; Schins, J. M.; Patil, S.; Scherf, U.; Siebbeles, L. D. A. High Intrachain Hole Mobility on Molecular Wires of Ladder-Type Poly(P-Phenylenes). *Phys. Rev. Lett.* **2006**, *96*, No. 146601, DOI: 10.1103/PhysRevLett.96.146601.
(26) Hummel, A. *Radiation Chemistry: The Chemical Effects of Ionizing Radiation and Their Applications*; Interfaculty Reactor Institute, Delft University of Technology: Delft, The Netherlands, 1995.
(27) Alig, R. C.; Bloom, S.; Struck, C. W. Scattering by Ionization and Phonon Emission in Semiconductors. *Phys. Rev. B: Condens. Matter Mater. Phys.* **1980**, *22*, 5565−5582.
(28) Infelta, P. P.; de Haas, M. P.; Warman, J. M. The Study of the Transient Conductivity of Pulse Irradiated Dielectric Liquids on a Nanosecond Timescale Using Microwaves. *Radiat. Phys. Chem.* **1977**, *10*, 353−365.
(29) Poborchii, V. V.; Kolobov, A. V.; Caro, J.; Zhuravlev, V. V.; Tanaka, K. Dynamics of Single Selenium Chains Confined in One-Dimensional Nanochannels of Alpo4−5: Temperature Dependencies of the First- and Second-Order Raman Spectra. *Phys. Rev. Lett.* **1999**, *82*, 1955−1958.
(30) Poborchii, V. V.; Kolobov, A. V.; Caro, J.; Zhuravlev, V. V.; Tanaka, K. Polarized Raman Spectra of Selenium Species Confined in Nanochannels of Alpo4−5 Single Crystals. *Chem. Phys. Lett.* **1997**, *280*, 17−23.
(31) Movaghar, B.; Sauer, G. W.; Würtz, D.; Huber, D. L. Time Decay of Excitations in the One Dimensional Trapping Problem. *Solid State Commun.* **1981**, *39*, 1179−1182.
(32) Movaghar, B.; Grünewald, M.; Pohlmann, B.; Würtz, D.; Schirmacher, W. Theory of Hopping and Multiple-Trapping Transport in Disordered Systems. *J. Stat. Phys.* **1983**, *30*, 315−334.
(33) Li, S. S. *Semiconductor Physical Electronics*; Springer: New York, 2006; DOI: 10.1007/0-387-37766-2.

DOI: 10.1021/acs.jpcc.7b05183
J. Phys. Chem. C 2017, 121, 18917−18921